

# The effects of ignored seabed variability in geoacoustic inversion

Anna-Liesa S. Lapinski<sup>a)</sup> and David M. F. Chapman  
*Defence Research and Development Canada—Atlantic, P.O. Box 1012, Dartmouth,  
Nova Scotia B2Y 3Z7, Canada*

(Received 3 November 2004; revised 24 March 2005; accepted 1 April 2005)

Geoacoustic inversion using a matched-field inversion algorithm is a well-established technique for estimating the geoacoustic parameters of the seabed. This paper demonstrates how parameter estimation can be affected by unknown or wishfully ignored random range dependence of the true environment when the inversion model is—for practicality—assumed to be range independent. Simulations with controlled statistics were carried out using a simple shallow water model: an isospeed water column over a homogeneous elastic halfspace. The inversion parameters included water depth, compressional speed in the seabed, seabed density, and compressional wave attenuation. On average the environment is range independent: some parameters are constant while other parameters are random with range-independent means and variances. A Parabolic Equation underwater acoustic propagation model is used to calculate the simulated data fields for the range-dependent environment as well as to calculate the model fields for the range-independent inversion model. The Adaptive Simplex Simulated Annealing inversion algorithm is used to estimate the best-fit solution. It is found that ignoring the variability of even a single geoacoustic parameter leads to significant and correlated uncertainty (bias and variance) in the estimation of all inverted parameters. Results are presented for range variation of compressional sound speed and water depth. [DOI: 10.1121/1.1921449]

PACS numbers: 43.30.Pc, 43.60.Kx [AIT]

Pages: 3524–3538

## I. INTRODUCTION

Geoacoustic inversion using a matched-field inversion (MFI) algorithm is a well-established technique for estimating the geoacoustic parameters of the seabed.<sup>1–9</sup> This paper demonstrates how parameter estimation can be affected by unknown or wishfully ignored random range dependence of the true environment when the inversion model is assumed to be range independent. A simple shallow water model is used for simulations with controlled statistics: the inversion parameters include water depth, seabed compressional speed, seabed density, and compressional wave attenuation. All environmental parameters are either assumed to be constant in range or random with range-independent means and variances. A Parabolic Equation underwater acoustic propagation model<sup>10</sup> is used to calculate both the simulated data fields for the range-dependent environment as well as the model fields for the range-independent inversion. It is found that ignoring the variability of even a single geoacoustic parameter leads to significant and correlated uncertainty (bias and variance) in the estimation of all inverted parameters.

Geoacoustic inversion is a technique used to determine geoacoustic properties in the ocean. When acoustic fields interact with the ocean environment, including the ocean bottom, they are influenced by properties of the environment. In the technique of geoacoustic inversion, measured geoacoustic fields  $\mathbf{d}$  are used to determine the  $M$  unknown parameters of a postulated model  $\mathbf{m} = \{m_i, i = 1, M\}$  that represents unknown geoacoustic properties of the ocean that have influ-

enced the measured field. The determination of  $\mathbf{m}$  using  $\mathbf{d}$  is the solution to the inverse problem.

The proper formulation of the inverse problem is imperative. If it is not formulated appropriately then the results of the inversion could be meaningless. In particular, determining a suitable model parametrization is an important preceding step to applying an inversion algorithm. *A priori* information about the ocean environment can help determine an appropriate model parametrization. When adequate information about the ocean environment is not available, techniques such as the underparametrized approach (e.g., as applied in Lapinski and Dosso<sup>11</sup> as well as Refs. 1 and 2) and the overparametrized approach used in conjunction with the inversion algorithm can be employed to determine the best model parametrization as well as  $\mathbf{m}$ . In this research, however, the goal was not to determine the best parametrization but rather to observe the effects of assuming a particular parametrization.

The research presented here is a documentation of some of the results from a single formulation of an inverse problem. It presents the results obtained by assuming that the unknown ocean bottom properties could be modeled as if they did not vary with range (i.e., they are range independent) while in reality the properties were randomly range dependent. Assuming the properties of the ocean environment can be treated as range independent is an appealing assumption in geoacoustic inversion because it can simplify the model parametrization and thereby can simplify the inversion. This paper considers how ocean bottom parameter estimation is affected by unknown or wishfully ignored random variation in certain environments.

<sup>a)</sup>Electronic mail: liesa.lapinski@drdc-rddc.gc.ca

Geoacoustic inversion is a nonlinear inverse problem. It has no direct solution. The technique of matched-field inversion is commonly used to ascertain a solution. In MFI, measured acoustic fields  $\mathbf{d}$  are compared with replica (modeled) acoustic fields  $\mathbf{d}(\mathbf{m})$  that have been generated using an acoustic propagation model with a proposed model  $\mathbf{m}$ . Typically, the goal of MFI is to minimize the objective function  $E(\mathbf{m})$ . To evaluate the proposed parameter values of the model  $\mathbf{m}$  an error function is defined that quantifies the mismatch between the measured field  $\mathbf{d}$  and the modeled field  $\mathbf{d}(\mathbf{m})$ . In this investigation, the objective function  $E(\mathbf{m})$  is the same as the error function. The error function used in this research is described in Sec. II B. Minimizing the objective function requires searching for the model that has the smallest mismatch  $E$ . Before the search begins, upper and lower bounds must be placed on each model parameter  $m_i^- < m_i < m_i^+$ . This defines the parameter space that is used in solving the inverse problem. The parameter space is then searched using an MFI algorithm to find the best model  $\mathbf{m}$ . The search can be a sizable activity. In geoacoustic inversion, many different MFI algorithms have been applied with varying success and efficiency.<sup>1-8</sup>

Given the variability that exists in the geoacoustic properties of the oceans, studying how well geoacoustic inversion techniques can be applied to range-dependent environments is a worthwhile endeavor. For example, in 2001 the Geoacoustic Inversion Techniques (GAIT) workshop was held to provide participants with an opportunity to apply their geoacoustic inversion techniques to range-dependent test cases.<sup>9</sup> The papers detailing the results of this workshop (including Ref. 9) are contained in a special issue of the *IEEE Journal of Oceanic Engineering* on geoacoustic inversion in range-dependent shallow-water environments. One reason to investigate the effect of ignoring range dependence is because if the range dependence can be ignored, less computationally intensive geoacoustic models can be employed in the inversions. Similarly, for the GAIT workshop data, Nielsen *et al.*<sup>12</sup> found that it was appropriate to apply both a Parabolic Equation (PE) based acoustic model (RAMGEO) and a (less-accurate; i.e., less computationally intensive) adiabatic model (PROSIM) to the data from the test case referred to as TC1. This could be done because the environment is only weakly range dependent: the environment is a smooth shallow-sloped downslope environment. The test case environment in TC3 is a simulation of an uplifted fault that consists of a rectangular intrusion of the basement material in the sediment layer. For TC3 the adiabatic model was thought to have failed due to the intrusion in the environment that caused significant mode coupling.<sup>12</sup> Only the PE acoustic model RAMGEO could be applied in this case. Also in that special issue, Harrison and Siderius<sup>13</sup> applied the “effective” water depth technique to two of the workshop test cases, the benefit being that a range-dependent environment can be replaced by a simplified equivalent range-independent environment for faster inversions. In other literature, Siderius *et al.*<sup>14</sup> safely neglected range dependence using a towed horizontal line array (HLA) and a towed source which in turn allowed for the neglect of range dependence during the inversions

while still allowing them to map a range-dependent environment.

In this paper the Adaptive Simplex Simulated Annealing (ASSA)<sup>1</sup> MFI algorithm is applied to synthetic geoacoustic data generated for an ocean environment that has one “unknown” ocean bottom property that varies with range. During the inversions a range-independent model is assumed. While studying the effect of ignoring range dependence, effects of simply applying the inversion algorithm should be kept in mind. Fallat *et al.*<sup>15</sup> investigated algorithm-induced variability for three geoacoustic inversion techniques, including ASSA. It was found that ASSA produced the lowest (i.e., best) objective function values and the lowest variability between inversion solutions for all environments it was applied to. However, it was noted that algorithm-induced variability should be evaluated on a case-by-case basis since the variability varied between test environments.

The goal of this paper is to investigate some of the effects of assuming a range-independent environment when performing an inversion. Section II introduces the environment, discusses ASSA and the error function used in this work, and introduces PE acoustic propagation models and the propagation model used in this investigation. Section III presents the results of the studies done for this investigation, which include results for an environment with range-dependent sediment compressional speed and for an environment with range-dependent water depth. Section IV summarizes the conclusions made.

## II. SETUP: MODELS AND ERROR FUNCTION

In the following the general environment is described, the ASSA algorithm is introduced, the error function used with the algorithm is discussed, and the acoustic propagation model used in this investigation is introduced.

### A. Environment

In order to look at the effect of ignoring range dependence when doing inversions, a prescribed ocean environment and “experimental setup” were first devised. The synthetic ocean environment used in this investigation is simple but realistic inasmuch as it is based on a model of the Sable Island Bank, which is part of the Scotian Shelf off the east coast of Canada where the ocean bottom consists of three general layers: sand and gravel over till over bedrock.<sup>16</sup> The simplified version of this environment used for this investigation, as seen in Fig. 1, consists of a water column over a semi-infinite layer of sand where water sound speed is  $V_w = 1460$  m/s,<sup>17</sup> water depth is  $H = 80$  m,<sup>18</sup> sediment density is  $\rho = 2.06$  g/cm<sup>3</sup>,<sup>17</sup> sediment attenuation coefficient is 0.26 dB/km Hz,<sup>17</sup> which gives an attenuation of  $\alpha_p = 0.436$  dB/ $\lambda$ , shear speed is  $V_s = 260$  m/s,<sup>19</sup> and shear attenuation is calculated to be  $\alpha_s = 2.6$  dB/ $\lambda$ .<sup>20</sup> The sediment compressional speed is taken as  $V_p = 1677$  m/s, the average of calculated sound speeds in Ref. 18 for the southern part of their survey area. That average has a standard deviation of  $\pm 71$  m/s, which put a maximum limit on how much the compressional speed could be allowed to vary in this investigation. The sediment compressional speed is realistic for

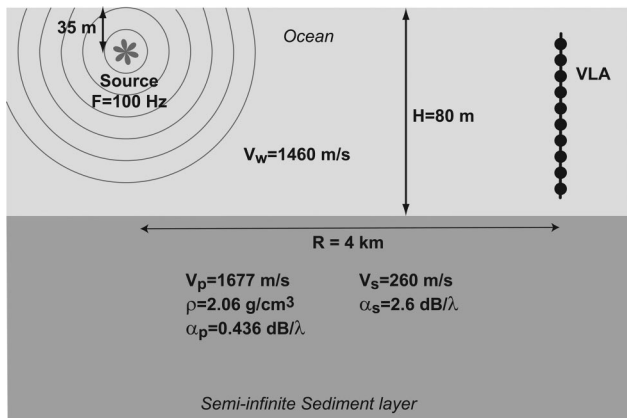


FIG. 1. Schematic representation of the basic ocean environment and “experimental setup” used for this study, including source frequency  $F$ , water sound speed  $V_w$ , water depth  $H$ , range  $R$ , sediment compressional speed  $V_p$ , sediment density  $\rho$ , compressional wave attenuation  $\alpha_p$ , shear speed  $V_s$ , and shear attenuation  $\alpha_s$ .

the Sable Island Bank in that it falls between general compressional speed values for “Sable Island Sand and Gravel.”<sup>19</sup>

A single source at 35 m depth and a vertical line array (VLA) with receivers every meter from 5 m depth to 75 m depth were used when generating the acoustic fields (Fig. 1). Typically, the source frequency was  $F = 100$  Hz and the range,  $R$ , from the source to the VLA was 4 km. In addition, to reduce model artifacts, such as unrealistic reflections from where the ocean bottom is terminated in the acoustic model, an absorbing bottom was included.

## B. Matched-field inversion

Optimizing through MFI methods requires the quantification of the difference between the measured and modeled data through an error function in order to evaluate the fitness of the model. The following starts by describing the error function followed by a brief description of the optimization algorithm applied here.

The essence of matched field techniques is that a field generated using a proposed model is compared to the actual measured field and then assessed. The difference between the fields (the fitness or mismatch) requires quantification using an error function. The general form of the error function  $E(\mathbf{m})$  used in this work for  $nF$  source frequencies and  $nS$  data snapshots (i.e., the number of data sets being used simultaneously in the inversion at source frequency  $F$ ) for observed data  $\mathbf{d} = \{\mathbf{d}_{ij}; i = 1 \dots nF; j = 1 \dots nS\}$  is

$$E(\mathbf{m}) = \sum_{i=1}^{nF} \sum_{j=1}^{nS} B_{ij}(\mathbf{m}) |\mathbf{d}_{ij}|^2 / v_{ij}, \quad (1)$$

where  $v_{ij}$  is the data variance and  $B_{ij}(\mathbf{m})$  is the normalized incoherent Bartlett mismatch. The normalized incoherent Bartlett mismatch has the formulation

$$B_{ij}(\mathbf{m}) = 1 - \frac{|\mathbf{d}_{ij}^\dagger(\mathbf{m}) \mathbf{d}_{ij}|^2}{|\mathbf{d}_{ij}|^2 |\mathbf{d}_{ij}(\mathbf{m})|^2}, \quad (2)$$

which can vary between 0 and 1 where 0 represents a perfect match (i.e., parallel vectors) and 1 represents a perfect mismatch (i.e., orthogonal vectors). Equation (1) is a form of the incoherent Bartlett processor. (It is more common to see it without the summation over data snapshots, for example as derived in Ref. 21.) The incoherent Bartlett processor is a common error function (also mismatch calculation) used for MFI of spatial acoustic-field data. It is a likelihood based processor derived when source amplitude and phase at each frequency are unknown. For a list of several other likelihood based processors see Refs. 21 and 22. The maximum likelihood model is found by minimizing Eq. (1) given the simplifying assumption that the measured data have complex, zero-mean, Gaussian-distributed random variable errors that are uncorrelated across space, frequency, and time, with identical variance at each array sensor.

Only relative values of the error function are important for optimization. If it can be assumed that  $|\mathbf{d}_{ij}|^2 / v_{ij}$  is constant with respect to frequency and snapshot then the error function [Eq. (1)] can be rewritten as

$$E(\mathbf{m}) = \frac{1}{nF \cdot nS} \sum_{i=1}^{nF} \sum_{j=1}^{nS} B_{ij}(\mathbf{m}), \quad (3)$$

which varies on  $[0,1]$ . Equation (3) is the error function used in this work.

The results contained in this paper, as with any data modeling investigation, depend in part on the particular error function used. It is possible that alternative results could have been obtained using a different error function. For example, Dosso and Wilmut<sup>21</sup> did a study on the effects of using different levels of information about the source amplitude and phase in MFI. They compared results obtained using three maximum likelihood processors and found that smaller parameter uncertainties were achieved if source information was used. The error function Eq. (3), which uses no source information, was chosen because often in MFI source spectrum information is not available and therefore these results would be of greater use. While the details of the results might change if a different error function was used, it would be expected that the general conclusions made here remain the same.

To perform the investigation reported in this work, the hybrid inversion algorithm ASSA<sup>1</sup> was used to minimize Eq. (3). A hybrid inversion method combines a local with a global inversion method in order to combine the strengths and alleviate the weaknesses of the two original methods. In this case, the local method of Downhill Simplex (DHS)<sup>23,24</sup> is combined with the global method of Simulated Annealing (SA).<sup>25,24</sup> The DHS component helps the algorithm converge upon an estimate of the global minimum in an efficient manner while the SA prevents the algorithm from getting stuck in suboptimal minima, and allows the parameter space to be widely searched. It has been shown to be an effective optimization algorithm<sup>1,11</sup> and has been applied to data from environments that have both range-independent<sup>1</sup> and range-dependent<sup>11</sup> properties. The reader is directed toward Ref. 1 if a description of the algorithm is required.

ASSA is an optimization algorithm. The error function Eq. (3) is used to help the algorithm evaluate the proposed

parameter models,  $\mathbf{m}$ , and subsequently ASSA minimizes Eq. (3). The model evaluation process in ASSA comes from the SA component of the algorithm. SA is based on the process of crystal growth through thermodynamic annealing. In the SA algorithm, the system (model) is repeatedly perturbed and the perturbations are accepted or rejected based on whether the perturbed system satisfies the METROPOLIS criterion<sup>26</sup>

$$\xi \leq \exp[-\Delta E/T], \quad (4)$$

where  $\Delta E$  is the difference between the energies (mismatches) of the proposed and current states (models),  $T$  is temperature (a control parameter) that decreases throughout the algorithm, and  $\xi$  is a uniform random number on  $[0,1]$ . Any perturbed system (model) that achieves a lower energy (mismatch) or in other words moves downhill in the objective function is accepted while a perturbed system (model) with a higher energy (i.e., moves uphill) may still be accepted. ASSA uses the METROPOLIS criterion to accept or reject perturbed models and for this investigation the mismatch,  $E$ , was calculated using the error function Eq. (3). To ensure that the best model possible is found, the final phase of the algorithm is a quenching that applies the pure DHS algorithm using the current best model found by applying ASSA. Without going into more algorithm detail, this is the underlying technique used to find the model with the lowest mismatch.

A detailed description of ASSA has not been presented here, but the values of certain ASSA parameters should be stated for the sake of the experimental setup used in this work. The ASSA control parameters mentioned here are discussed more fully in Refs. 1 and 2. One set of control parameters, the annealing schedule, consists of the starting temperature  $T_0$  [where the temperature  $T$  is the parameter defined in Eq. (4)], the rate of reducing the temperature  $\beta$  ( $\leq 1$ ), the maximum number of temperature steps, and the number of accepted perturbations at each temperature step. (The actual number of temperature steps varied with each application of ASSA because a convergence criterion was enforced prior to quenching so that computation time was not wasted.) In general, the larger the annealing parameter values are the slower and more extensive the exploration of the search space is. The difficulty of the inversion problem defines how intensive a search should be conducted. Some initial runs with different annealing schedules are usually required to find a schedule that generates results that cannot be appreciably improved by intensifying the search. The annealing schedule used in this work was typically  $T_0=0.7$ ,  $\beta=0.975$ , 5 accepted perturbations, and a maximum of 400 temperature steps. In certain studies, when it was noted that the algorithm was having problems converging prior to quenching, the annealing schedule had to be altered: the maximum number of temperature steps went up to 600 and the number of accepted perturbations reached 7. The changes intensified the search. In addition to these parameters, the Cauchy distribution parameters<sup>1</sup>  $S$  and  $s$ , which influence the adaptive nature of the algorithm, were set to  $S=30$  and  $s=3$ .

### C. Setup of the propagation model PECan

Matched-field inversion requires the calculation of the acoustic fields at the receivers given the proposed model in order to evaluate the model using an error function. There are a variety of types of acoustic propagation models that can be used to calculate acoustic fields. The PE method is the method used here because it can be used to calculate fields in both range-independent and range-dependent environments. When calculating fields for range-dependent environments the PE method can be less computationally intensive than some other methods, such as the coupled-modes method. The particular propagation model used here is PECan.<sup>10</sup> This section describes the problem-specific setup of PECan along with a feature of PECan that was utilized to help generate the continuously variable properties.

PECan was used to calculate the “measured” fields  $\mathbf{d}$  and the replica fields  $\mathbf{d}(\mathbf{m})$  needed to evaluate the model. While a range-independent environment was assumed during the inversions, to calculate  $\mathbf{d}$  an acoustic model that could handle range dependence was also needed. There can be differences between an acoustic field calculated using different acoustic propagation models. The significance of these differences depends on what the calculated acoustic field is used for. To minimize consequential numerical errors between the “measured” and replica fields, i.e., numerical differences that could affect conclusions, PECan was used to calculate both the fields. Due to the far-field approximation made in PE models, the VLAs were also placed well in the far-field, several kilometers from the source.

The accuracy and computation time of a PE model can be affected by choices made during the setup of the model. To solve a parabolic equation, the environment is divided laterally ( $\Delta r$ ) and vertically ( $\Delta z$ ). Using a split-step Padé solution method, larger range steps can be used compared to other PE solution methods thereby reducing the computation time.<sup>10</sup> Finding the appropriate grid size to use when calculating an acoustic field is an important step. Finer grids provide a more accurate solution but require larger computations. For inversion purposes it is therefore important to strike a balance between grid size and the accuracy needed. A similar time versus accuracy balance is needed for the feasible number of Padé expansion terms ( $N_p$ ): computations increase as the number of expansion terms (accuracy) increase.

PECan has many options and parameters that must be set prior to applying the model. For the inversions in this investigation an analytic Green’s starting field, the energy-conservation option, and the split-step Padé solution method were used. The PECan parameters that needed to be defined for the inversions were the values of the grid spacing  $\Delta z$  and  $\Delta r$ , the depth at which the absorbing bottom starts  $H_a$ , and the number of Padé terms  $N_p$ . The thickness of the absorbing bottom  $\Delta H_a$  also needed to be determined.

To determine the appropriate PECan parameter values one realization of an ocean environment based on Fig. 1 with variable compressional speed  $v_p(x)$  was created (more details on how variability was introduced are discussed in the following section). The choice of value for  $\Delta z$ ,  $\Delta r$ ,  $H_a$ ,  $\Delta H_a$  and  $N_p$  contributes to how computationally intensive

TABLE I. Results of PECan parameter studies. For 25, 50, 100, and 200 Hz data the chosen  $\Delta z$ ,  $\Delta r$ ,  $N_p$ ,  $H_a$  ( $H_a$  is a depth measured from the ocean surface) and  $\Delta H_a$  are included.

Frequency (Hz)	$\Delta z$ (m)	$\Delta r$ (m)	$N_p$	$H_a$ (m)	$\Delta H_a$ (m)
25	1.0	40	3	400	100
50	0.4	50	3	140	50
100	0.25	8	3	110	100
200	0.125	10	4	90	10 <sup>a</sup>

<sup>a</sup>Some inversions were done with a  $\Delta H_a = 100$  m.

each call to PECan will be during the inversions. Appropriate values for each parameter were determined in the following way: A “true” field was first generated using a computationally intensive set of PECan parameter values. Without changing the environment, with the exception of the artificial absorbing layer, PECan was repeatedly run using all possible combinations of a selection of PECan parameter values. The calculated (replica) fields were compared to the originally generated “true” field using the error function in Eq. (3) with  $nF=1$  and  $nS=1$ . From these results, a set of PECan parameter values that gave an acceptable mismatch and an acceptable computational time was chosen. An acceptable mismatch was a comparative value based on the best mismatches achieved for the PECan parameters combinations. A mismatch less than  $10^{-4}$  was acceptable but a mismatch close to machine precision was desirable. An acceptable computational time for the forward propagation model was again a comparative value based on the computation times for each combination of PECan parameter values. On a PC with a 2 GHz CPU, a few seconds or less was desirable. The process of determining the best parameter values had to be repeated for each source frequency used in this investigation, which included 25, 50, 100, and 200 Hz. The PECan parameter values picked for each frequency are quoted in Table I.

Another of PECan’s features was utilized to help create the continuously variable ocean environments used in this investigation when calculating  $\mathbf{d}$ . In PECan the environment is defined using environmental profiles. PECan allows for linear interpolation between environmental profiles. The range-dependent properties for environmental profiles with range variability were specified at evenly spaced range points, and PECan linearly interpolated between each profile as illustrated for variable compressional speed in Fig. 2. The

linear interpolation feature was employed so that the variability was continuous with range within the limit of the grid spacing.

### III. RESULTS

In this section the method of investigation is explained and the results are presented. The inversion results have been grouped into studies. For each study the “experimental setup” was established and the range-dependent variability had a prescribed mean and standard deviation. Typically, 100 inversions were performed per study. Unless stated otherwise, the true environment used to generate the “measured” field  $\mathbf{d}$  had a different realization of the range-dependent variability for each inversion in the study. This corresponds to doing inversions using data from multiple tracks for a certain ocean environment. The spread and correlations of the optimal model parameter solutions found through the inversions could then be examined and compared within and between the studies.

When ASSA was applied it was assumed that the “unknown” ocean bottom properties could be modeled as range independent. A four-parameter model was inverted for in the inversions. The parameters represented water depth  $H$ , sediment compressional speed  $V_p$ , density  $\rho$ , and attenuation  $\alpha_p$ . The shear speed  $V_s$  and attenuation  $\alpha_s$  were assumed to be known and constant. When generating the “measured” field  $\mathbf{d}$ , prior to the inversion, the true values of the model parameters were those quoted in Fig. 1, except, of course, for the property that varied with range in the particular study. The results presented in the following sections include results for variable compressional speed and variable water depth.

The shear parameters were held constant to reduce the dimensionality of the problem. Even without environmental variability, there is ambiguity among the geo-acoustic parameters of this simple model.<sup>27</sup> It will be shown that when shear parameters are held constant, the inversion (when successful) consistently finds correct parameter values when the environment does not vary. This provides a good baseline case for reference purposes, with no inherent ambiguity. More complex cases of multiple range-dependent parameters could be a topic of further study, using the current work as a starting point.

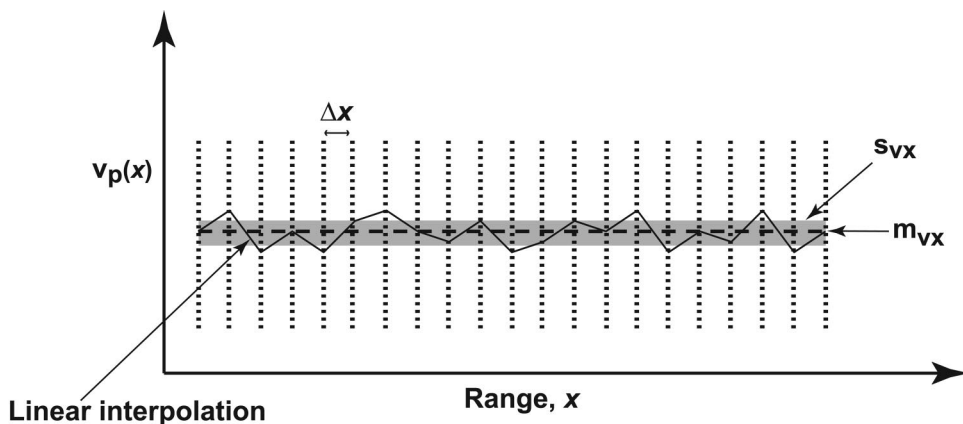


FIG. 2. Schematic representation of the compressional speed variability. The horizontal axis represents range  $x$  and the vertical axis represents the variable compressional speed  $v_p(x)$ . The dotted vertical lines represent where the PECan environmental profiles are defined, which is every  $\Delta x$  interval. PECan linearly interpolates between where the fluctuations are defined. The resulting linearly interpolated range-dependent profile has a set mean  $m_{vx}$  and standard deviation  $s_{vx}$ .

## A. Variable compressional speed

The sediment compressional speed was one of the ocean bottom properties that was allowed to vary with range  $v_p(x)$  in this investigation. To create  $v_p(x)$ , fluctuations were generated using scaled pseudorandom numbers picked from a uniform distribution. For  $N+1$  environmental profiles defined in PECan (i.e.,  $N$  segments),  $N+1$  fluctuations were

$$m_{vx} = \frac{1}{2N} \sum_{i=0}^N ([v_p]_{i+1} + [v_p]_i), \quad (5)$$

$$s_{vx} = \pm \sqrt{-m_{vx}^2 + \frac{1}{3N} \sum_{i=0}^N ([v_p]_{i+1}^2 + [v_p]_i^2 + [v_p]_{i+1}[v_p]_i)}. \quad (6)$$

For a derivation of Eqs. (5) and (6) please refer to Appendix A.

Table II summarizes the features of each study presented here for variable compressional speed (studies V1–V8). Four studies include inversions for 100 Hz source frequency (V1–V4) while the others include source frequencies of 25, 50, and 200 Hz (V5, V6, and V7, respectively) and multiple source frequencies 100 and 200 Hz (V8). For some numerical propagation models, such as the one used here, the computational effort to calculate the field prohibitively increases with increasing frequency. Studies using frequencies higher than 200 Hz were not attempted due to the computation time that inversions at those frequencies require. For all studies

TABLE II. Summary of characteristics of each study presented in this paper. The data include the study number, the number of realizations of the ocean bottom used  $N_R$ , the number of inversions performed in the study  $N_I$ , the number of source frequencies used  $N_F$ , the source frequencies used  $F$ , the range between source and VLA  $R$ , and standard deviations of compressional speed variability  $s_{vx}$  and water depth variability  $s_{hx}$ .

Study number	$N_R$	$N_I$	$nF$	$F$ (Hz)	$R$ (km)	$s_{vx}$ (m/s) for $v_p(x)$
A	1	29	1	100	4	0
V1	100	100	1	100	4	$\pm 5$
V2	100	100	1	100	4	$\pm 20$
V2(a)	1	31	1	100	4	$\pm 20$
V2(b)	1	31	1	100	4	$\pm 20$
V3	100	100	1	100	4	$\pm 40$
V4	100	100	1	100	15	$\pm 20$
V5	100	100	1	25	4	$\pm 20$
V6	100	100	1	50	4	$\pm 20$
V7	100	100	1	200	4	$\pm 20$
V8	100	100	2	100, 200	4	$\pm 20$

Study number	$N_R$	$N_I$	$nF$	$F$ (Hz)	$R$ (km)	$s_{hx}$ (m) for $h(x)$
H1	100	100	1	100	4	$\pm 0.125$
H2	100	100	1	100	4	$\pm 0.250$
H3	100	100	1	100	4	$\pm 0.500$
H4	100	100	1	100	4	$\pm 0.750$
H5	100	100	1	100	4	$\pm 1.000$

generated to form a set of fluctuating compressional speed values  $\{[v_p]_i, i=0, N\}$ . These values were assigned to the  $N+1$  environmental profiles and PECan was allowed to linearly interpolate between the profiles to create  $v_p(x)$  (Fig. 2). For variable compressional speed, the environmental profiles were 100 m apart. Fluctuations were generated so that  $v_p(x)$  would have a set (true) mean  $m_{vx} = 1677$  m/s and standard deviation  $s_{vx}$  as defined by

except study V8,  $nF = 1$  and  $nS = 1$  in Eq. (3). For study V8,  $nF = 2$ .

For study V1 (Table II), the true environments had a range-dependent compressional speed  $v_p(x)$  with a standard deviation of  $s_{vx} = \pm 5$  m/s about a mean  $m_{vx} = 1677$  m/s. Figures 3(i)–3(l) are plots of the mismatches of the 100 inversion solutions versus the model parameter results. As can be seen in Figs. 3(i)–3(l), solutions that achieved a mismatch below  $\sim 6 \times 10^{-4}$  are clustered about the true mean  $m_{vx}$  or true values used to generate the environments. However, for all four model parameters, if the inversion result had a mismatch greater than  $\sim 6 \times 10^{-4}$  a wider distribution of results not centered about the true values or true mean value was obtained.

For comparison, Fig. 4 is a plot comparable with Figs. 3(i)–3(l). It too is a plot of mismatch versus inversion result; however, for these inversions the true environment was actually a range-independent environment as shown in Fig. 1 (study A, Table II). Twenty-nine inversions were performed, and most of the inversion results (21 of them) were tightly clustered about the true parameter values. These 21 results all had mismatches of  $\sim 10^{-7}$ ; in other words the mismatch achieved 0 for the given machine precision. The remaining inversion results converged to suboptimal solutions and were not scattered about the true values. This figure shows how tight a cluster about the true solution can be achieved and that the inversion algorithm does not always find the best solution. A possible reason for the latter observation is that the inversion algorithm, as it was set up for this investigation, did not search the search space as thoroughly as it should have. Therefore, for the data shown in Figs. 3(i)–3(l) there are two possible reasons for the suboptimal results: for those environments either no significantly better model result existed (i.e., a result with a significantly lower mismatch did not exist) or the algorithm's search was unsuccessful. Regarding the latter possibility, inversion results in this study are not guaranteed to be optimal, despite having acceptable control parameters. Nevertheless, the general trends which lead to the conclusions of this study are still evident even in the presence of a small segment of outliers, which are less

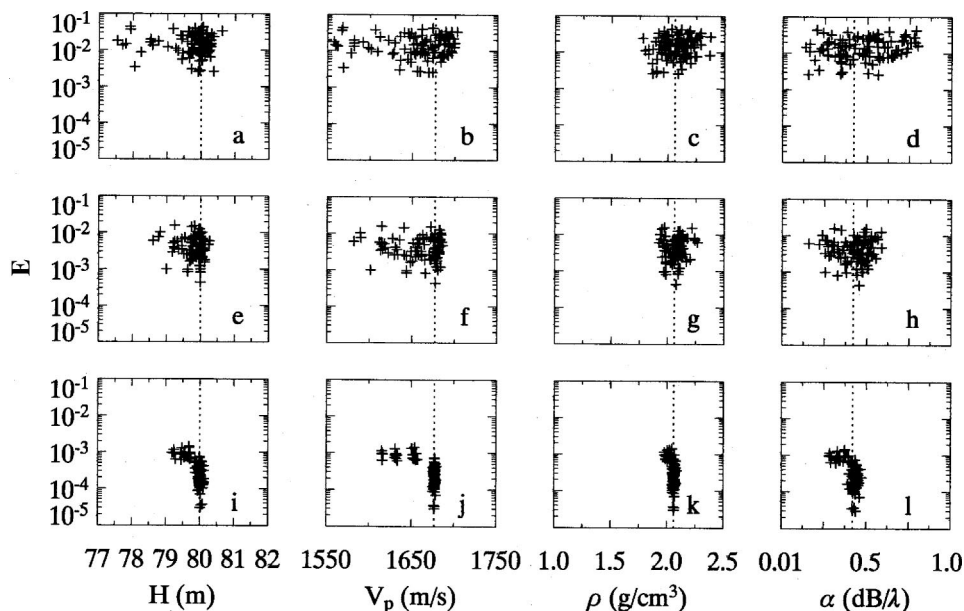


FIG. 3. Mismatch vs model parameter values for the solution sets of studies V3 ( $s_{v,x} = \pm 40$  m/s) are shown in (a)–(d), V2 ( $s_{v,x} = \pm 20$  m/s) are shown in (e)–(h), and V1 ( $s_{v,x} = \pm 5$  m/s) are shown in (i)–(l). The model parameters include water depth  $H$ , compressional speed  $V_p$ , density  $\rho$ , and attenuation  $\alpha$ . For  $H$ ,  $\rho$ , and  $\alpha$  the vertical dotted lines represent the true model parameter values used to generate the measured acoustic field, and for  $V_p$  it represents the  $m_{v,x}$ . The abscissa limits represent the bounds used in the inversions.

noticeable in the range-dependent environments.

Figures 3(a)–3(d) and 3(e)–3(h) show results for studies with variable compressional speed that have standard deviations of  $s_{v,x} = \pm 20$  m/s [study V2, Figs. 3(e)–3(h)] and  $s_{v,x} = \pm 40$  m/s [study V3, Figs. 3(a)–3(d)]. As can be seen, as the variability increases, the average mismatch increases as does the spread of solutions. It is likely that the average mismatches increase because there is no model that exists in the search space that can generate a replica field that is close to the “measured” field. Looking at Figs. 3 and 4, it appears that as more variability is added, the depth of the global minimum for all environments shrinks until there is no global minimum at the true parameter values and the true mean  $m_{v,x}$ .

To again look at how predictable the results of the inversions were, two sub-studies were done for study V2 [see Table II, studies V2(a) and V2(b)]. Two realizations of the ocean environment were chosen out of the original V2 study, and multiple inversions were performed on the fields generated from those environments. The results of those inversions are found in Fig. 5. As can be seen, for the environment that produced the results in Figs. 5(a)–5(d) there appeared to be a global minimum in the objective function at the true mean  $m_{v,x}$  and true parameter values, however for some of the inversions a good estimate of the global minimum was not located. For the environment represented by Figs. 5(e)–

5(h) there does not appear to be a well-defined global minimum. Except for density  $\rho$ , a spread of values at approximately the same mismatch was found. Therefore, for an environment that does not have a well-defined global minimum the result from a single inversion will likely be just one of many equally good solutions. The environment for study V2(b) [Figs. 5(e)–5(h)] could lack a well-defined optimal solution but the environment for study V2(a) [Figs. 5(a)–5(d)] seems to have a well-defined optimal solution.

The spread and concentrations of the  $s_{v,x} = \pm 5$  m/s,  $\pm 20$  m/s, and  $\pm 40$  m/s data (studies V1, V2, and V3) are better seen in Figs. 6(j)–6(l), 6(e)–6(h), and 6(a)–6(d), respectively. Figure 6 presents histogram plots of the results for each study. If one assumes a range-independent environment while performing an inversion, it can be seen that for small variations, like  $s_{v,x} = \pm 5$  m/s, one is likely to obtain a solution close to the true and true mean values. In Figs. 6(j) and 6(k) a high concentration of the model parameter values were clustered tightly about  $m_{v,x}$  and the true  $\rho$  value, respectively. It can be concluded that for the general environment used in this investigation, if the variability is small, one is likely to find a solution that represents the true environment after performing only one inversion. As the variability increases, the solutions found by single inversions of the environment are increasingly unreliable estimates of the true environment. This is reminiscent of adding increasing amounts

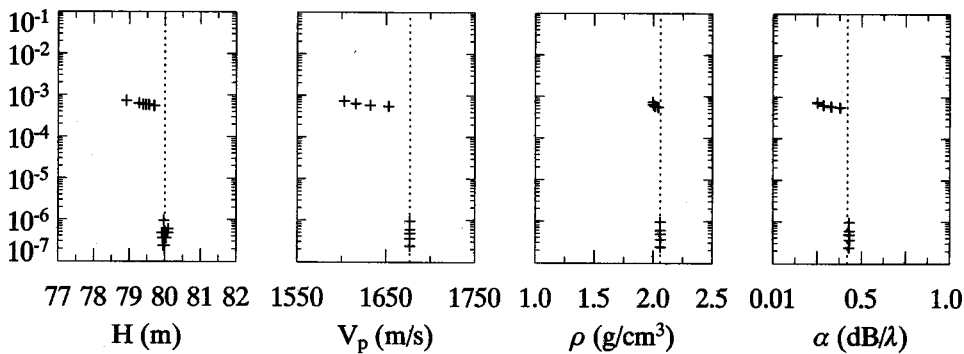


FIG. 4. Mismatch vs model parameter values for the solution set of study A. The true environment for this study is range independent (i.e., no parameter fluctuations have been added). The model parameters, abscissa limits, and vertical dotted lines are as described in Fig. 3.

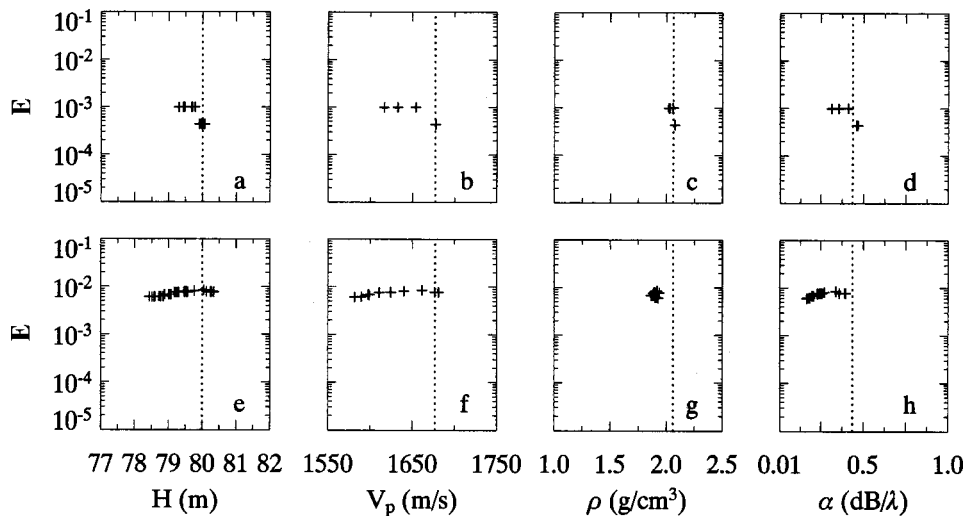


FIG. 5. Mismatch vs model parameter values for inversion solutions for studies V2(a) shown in (a)–(d) and V2(b) shown in (e)–(h) are presented ( $s_{vx} = \pm 20$  m/s). For each study, a unique range-dependent environment was used. The model parameters, abscissa limits, and vertical dotted lines are as described in Fig. 3.

of noise to synthetic noise-free acoustic data, which can reduce the precision at which model parameters can be determined.<sup>1,28</sup>

The effect of environmental variance of sediment sound speed is striking. The value  $|s_{vx}| = 40$  m/s is low compared to reported natural variations in surficial sound speed in shallow water. McKay *et al.*<sup>18</sup> reported standard deviations of sound speed of 71 m/s over hundreds of kilometers on the Scotian shelf, while Mayer *et al.*<sup>29</sup> measured a sound speed range of 277 m/s in the ONR Geoclutter area, even measuring a difference of 118 m/s between stations less than 1 km apart. (No standard deviations were published.) Lepage<sup>30</sup> found strong effects in propagation and reverberation model results from an input sound speed variation of 20 m/s. The results in this paper show that inversions in environments with typical values of sound speed variance lead to significant uncertainty in all estimated parameter values, when environmental variability is ignored.

It is also informative to look at the correlations between parameters. Figures 7–9 show two-dimensional correlation scatter plots for studies V1, V2, and V3, respectively. As

seen earlier, in study V1 for  $s_{vx} = \pm 5$  m/s there are groups of results about  $m_{vx}$  and the true model parameter values but there are also other solutions away from those values. Those other solutions typically have lower values than  $m_{vx}$  or the true parameter values. It can also be seen that the results are highly correlated between parameters. In Fig. 8, the V2 study data for  $s_{vx} = \pm 20$  m/s are presented. The parameters are no longer as highly correlated with the exception of  $V_p$  and  $H$ . The spreads of the results have increased but there are still solutions clustered about  $m_{vx}$  and the true parameter values, as seen earlier in Figs. 6(e)–6(h). Like for the V1 study, the inversion solutions for  $V_p$  and  $H$  are not likely to be greater than  $m_{vx}$  and the true  $H$  parameter value. In Fig. 9, the V3 study data for  $s_{vx} = \pm 40$  m/s are presented. In this figure, the distributions of the inversion results have increased again. There is no cluster about  $m_{vx}$  or the true  $\alpha$  parameter value. However,  $V_p$  and  $H$  are still highly correlated. The strong correlations between inverted parameters suggest that for moderate data/model mismatch, there is an ambiguity between members of a family of models, where each model in

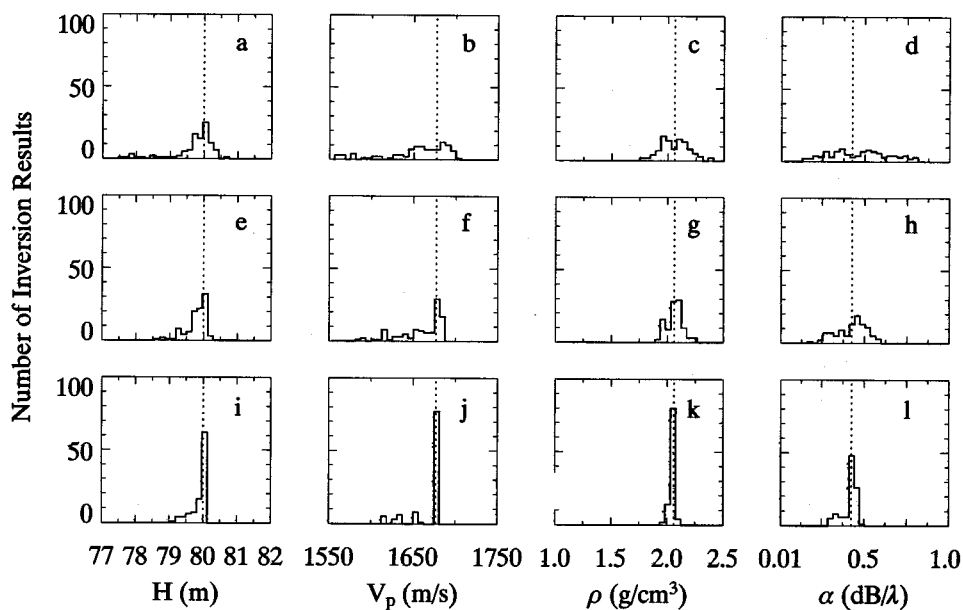


FIG. 6. Comparing different  $s_{vx}$  through histograms. The histograms of the inversion results for studies V1 (i)–(l), V2 (e)–(h), and V3 (a)–(d) are presented. The inversion results include model parameter values for water depth  $H$ , compressional speed  $V_p$ , density  $\rho$ , and attenuation  $\alpha$ . For  $H$ ,  $\rho$ , and  $\alpha$  the vertical dotted lines represent the true model parameter values used to generate the measured acoustic field, and for  $V_p$  it represents the  $m_{vx}$ . The abscissa limits represent the bounds used in the inversions.

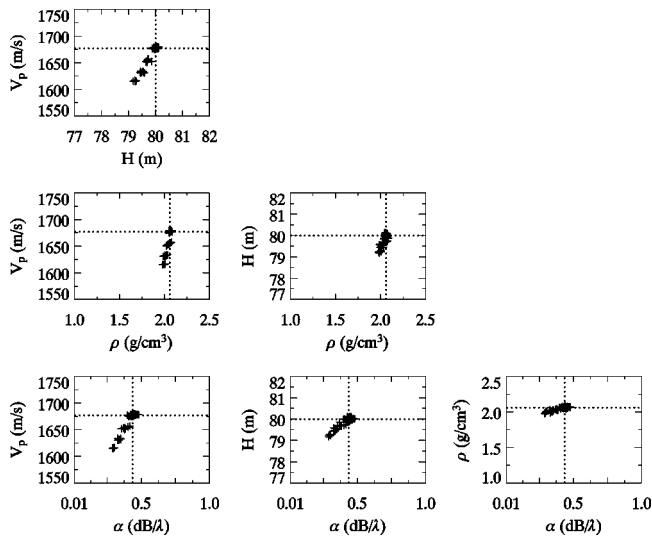


FIG. 7. The two-dimensional correlation scatter plots for the inversion solutions of study V1. The inversion results include model parameters values for  $H$ ,  $V_p$ ,  $\rho$ , and  $\alpha$ . For  $H$ ,  $\rho$ , and  $\alpha$  the dotted lines represent the true model parameter values used to generate the measured acoustic field, and for  $V_p$  it represents the  $m_{v,x}$ .

a family has a similar net effect on the acoustic field. In other words, the inversion has found a family of “effective” or nearly “equivalent” seabed models, as described by Chapman.<sup>27</sup> As the environmental variability increases, the data/model mismatch becomes greater, and the correlation worsens. Again, for water depth and compressional speed, parameter values above certain values are still not accepted.

To examine the effect of different values of  $R$  on the inversion results, a study similar to V2 was done using a range of 15 km (study V4) rather than 4 km. The standard deviation of the variability was  $s_{v,x} = \pm 20$  m/s. The results of study V4 are shown in Figs. 10(a)–10(d) along with the comparable V2 results in Figs. 10(e)–10(h). Between these ranges, the overall differences are few. The values of  $H$  and  $V_p$  have higher variances at the longer range and are skewed

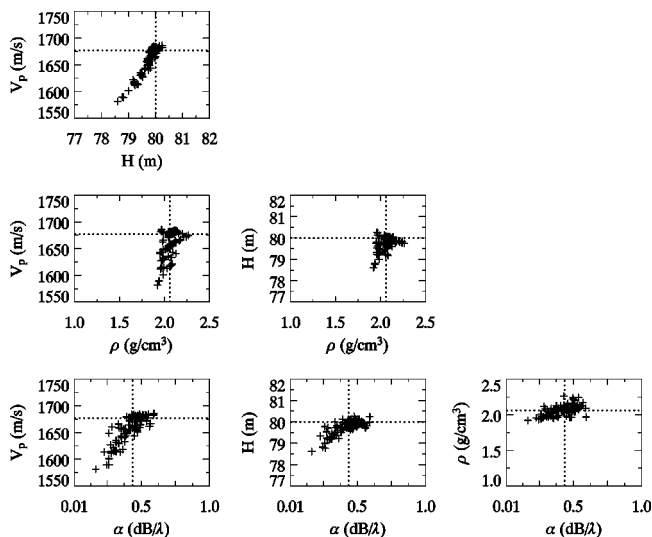


FIG. 8. The two-dimensional correlation scatter plots for the inversion solutions of study V2. The inversion results include model parameters values for  $H$ ,  $V_p$ ,  $\rho$ , and  $\alpha$ . The dotted lines are as described in Fig. 7.

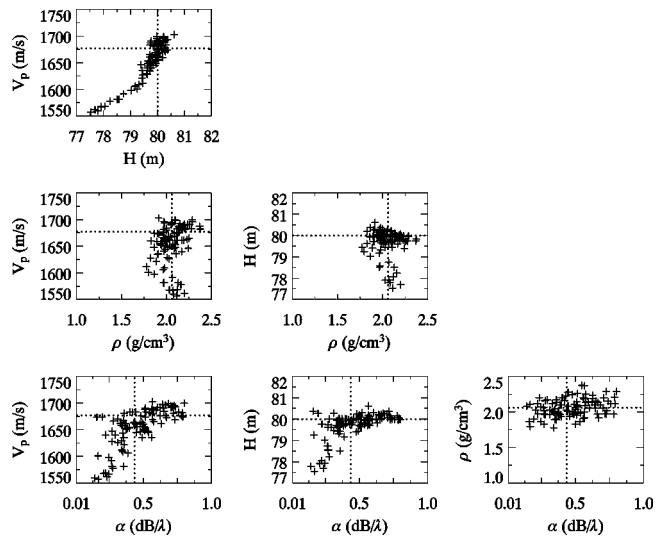


FIG. 9. The two-dimensional correlation scatter plots for the inversion solutions of study V3. The inversion results include model parameters values for  $H$ ,  $V_p$ ,  $\rho$ , and  $\alpha$ . The dotted lines are as described in Fig. 7.

above the true mean values. This implies that the acoustic field is less complex at longer range, providing less independent information across the array of sensors. Another possibility is that the effects of the variable environment accumulate with range, making the data fields more noise-like, which can make precisely determining the true and true mean parameter values more difficult.

Similar studies to V2 were also performed using different source frequencies  $F$ . The results are shown in Fig. 11 through histogram plots. Figure 11 presents data for studies V5, V6, V2, and V7 (Table II) which have source frequencies  $F = 25, 50, 100,$  and  $200$  Hz, respectively. For these studies  $R = 4$  km and  $s_{v,x} = \pm 20$  m/s. It should be noted that for the 200 Hz study (V7) the thickness of the false bottom was changed during the study. It was determined that a 10 m absorbing layer thickness ( $\Delta H_a$ ) was equivalent to a 100 m thickness. This change decreased the computational time of each call to PECAN. The inversion results for the 25 and 50 Hz data [Figs. 11(m)–11(p) and 11(i)–11(l), respectively] show no preference for any particular model parameter values. This is probably due to the lack of information available in the acoustic fields. Drawing from normal mode theory, the 25 Hz source has one trapped mode traveling through the environment. The 50 Hz source has approximately three trapped modes. Due to the simplicity of the acoustic fields, it is perhaps logical that the fields do not have enough information to help the inversion algorithm determine the appropriate model parameters for this environment. For 200 Hz source data [Figs. 11(a)–11(d)], the clustering about  $m_{v,x}$ , and the true parameter values of  $H$  and  $\rho$  are more pronounced than the 100 Hz results [Figs. 11(e)–11(h)]. These results imply that the complexity of the acoustic field increases with frequency, at least for this simple single-layer model. Consequently, at the higher frequencies, the data at different sensors would be more independent, while at low frequencies the data would be more correlated across the

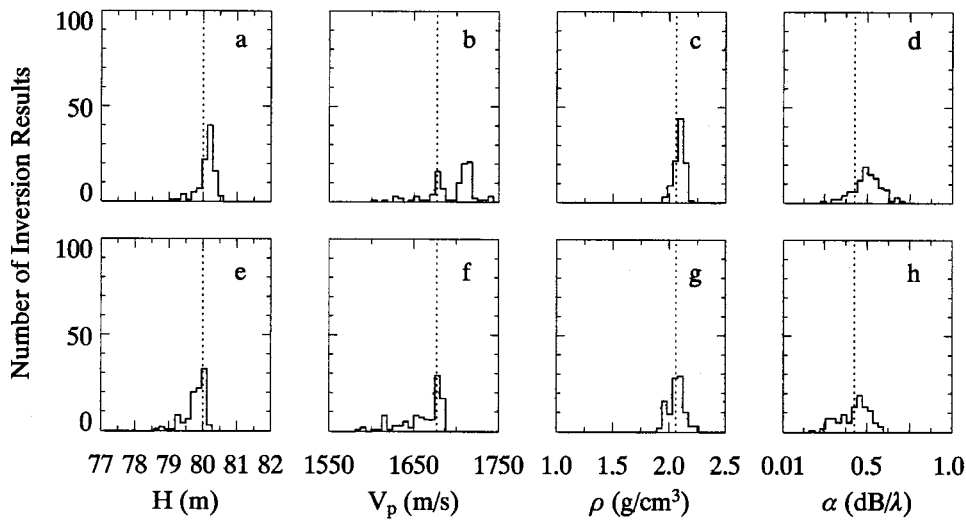


FIG. 10. Comparing different ranges. The histograms of the inversion results for studies V4 ( $R=15$  km) shown in (a)–(d) and V2 ( $R=4$  km) shown in (e)–(h) are presented. The inversion results include model parameter values for  $H$ ,  $V_p$ ,  $\rho$ , and  $\alpha$ . The vertical lines and abscissa limits are as described in Fig. 6.

array. In Fig. 11, even with ignored variability, the uncertainty in the model parameters seems to decrease at higher frequencies; however, this may not be the case for multilayer environments, in which the high frequencies naturally would be more sensitive to the parameters of the upper layers than those of the deeper layers.<sup>31–33</sup> The effects of ignored variability on multilayer inversion are proposed as a topic of further study, along with the potential remedy of multifrequency inversion.

Finally, with respect to variable compressional speed, a multiple source frequency study was completed (study V8), i.e., a study in which “measured” acoustic data from more than one source frequency was used at the same time to do the inversion. The source frequencies of 200 and 100 Hz were used. Figure 12 shows the histogram results of study V8 with other comparable single source frequency results. The single frequency results shown in Fig. 12 are for  $F=100$  Hz [Figs. 12(i)–12(l)] and for  $F=200$  Hz [Figs. 12(e)–12(h)]. It can be seen, in comparison to the single frequency results, that the algorithm was more successful at converging to the true parameter values for  $\rho$  and  $H$  when the

multiple frequencies were used. Approximately 90% of the predicted  $H$  parameter values were very near the true value. This encouraging result suggests that multifrequency inversion provides a partial remedy for uncertainty in inversion parameters in problems with ignored seabed variability, a possible topic for future work.

Table III states the mean of the inversion solution parameter values for the variable properties for each of the studies. As can be seen from Table III, the true mean of the studies,  $m_{v_x}$ , always fell within one standard deviation of the mean of the inversion solution values for each study. However, there was considerable difference from study to study between the values of  $s_{NV}$ , the standard deviation of the model parameter values for compressional speed, as would be expected from the results. It should be noted that care should be taken in comparing  $s_{NV}$  to  $s_{v_x}$  (Table II). The values of  $s_{v_x}$  are the standard deviations about  $m_{v_x}$  which was used to generate range-dependent variability while  $s_{NV}$  are standard deviations of the respective samples of solutions for compressional speed about the sample mean.

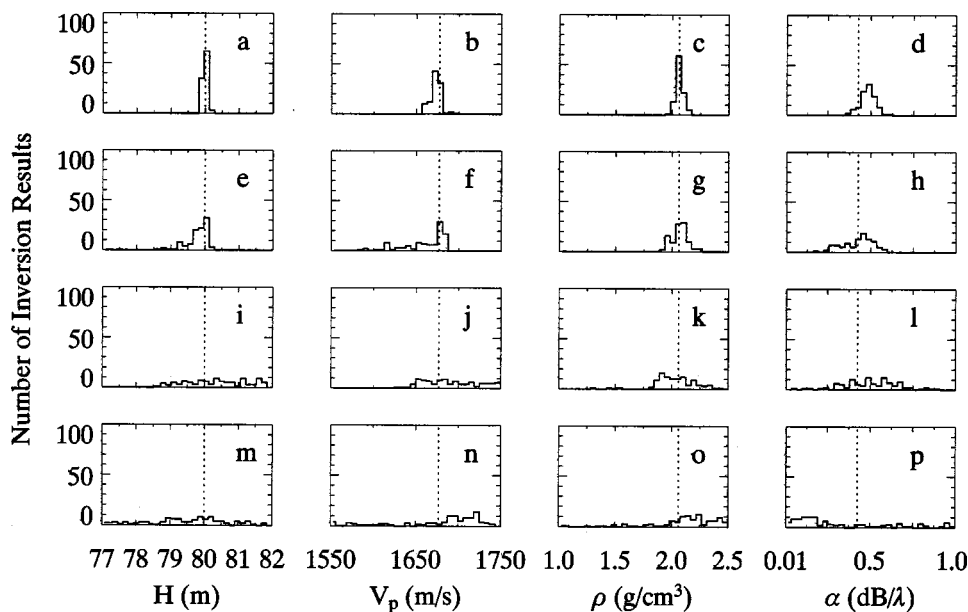


FIG. 11. Comparing different frequencies. The histograms of the inversion results for studies V7 ( $F=200$  Hz) shown in (a)–(d), V2 ( $F=100$  Hz) shown in (e)–(h), V6 ( $F=50$  Hz) shown in (i)–(l), and V5 ( $F=25$  Hz) shown in (m)–(p) are presented. The inversion results include model parameter values for  $H$ ,  $V_p$ ,  $\rho$ , and  $\alpha$ . The abscissa limits represent the bounds used in the inversions. The vertical lines and abscissa limits are as described in Fig. 6.

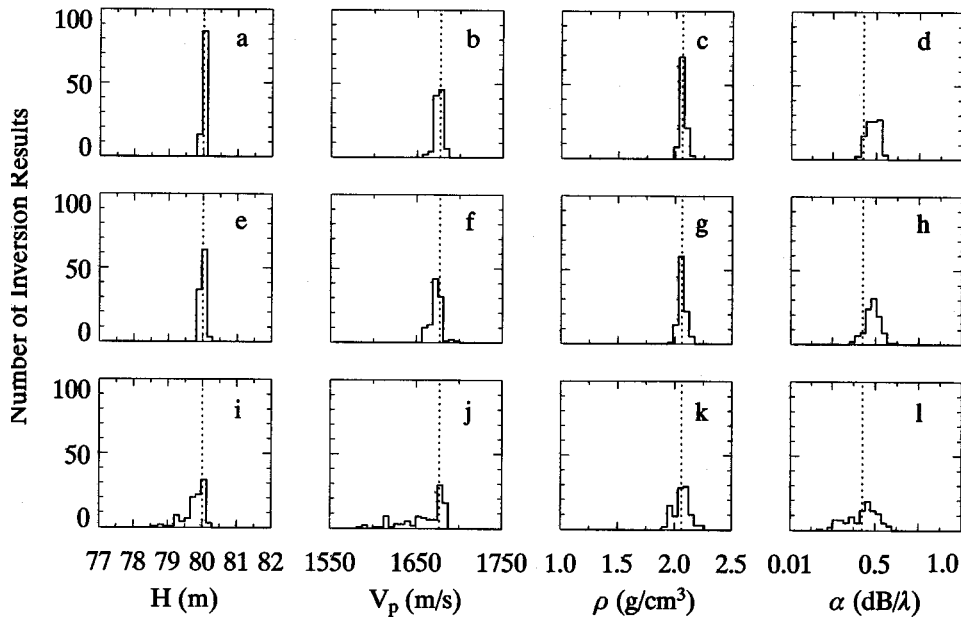


FIG. 12. Looking at multiple frequency inversion. The histograms of the inversion results for studies V8 ( $F=100$  and  $200$  Hz) shown in (a)–(d), V7 ( $F=200$  Hz) shown in (e)–(h), and V2 ( $F=100$  Hz) shown in (i)–(l) are presented. The inversion results include model parameters values for  $H$ ,  $V_p$ ,  $\rho$ , and  $\alpha$ . The vertical lines and abscissa limits are as described in Fig. 6.

### B. Variable water depth

Similar to the studies done for variable compressional speed, studies were also done for variable water depth  $h(x)$ . The features of the studies H1–H5 referred to in this work for variable water depth are summarized in Table II. The source frequency used was  $100$  Hz and the range between source and receiver was  $4$  km. Like for variable compressional speed, the mismatches were calculated using Eq. (3), with  $nF=1$  and  $nS=1$ . For studies H1–H5,  $100$  inversions were completed for each study, each inversion using a unique realization of the ocean bottom.

To generate the variable water depths, a combination of sine waves with random phases was used to create smooth and realistic variability. See Appendix B for the details of how the variability was created. For  $N+1$  environmental

profiles defined in PECAN,  $N+1$  water depth points were generated using the method described in Appendix B to form a set of values  $\{[h]_i, i=0, N\}$ . These values were assigned to the  $N+1$  environmental profiles and PECAN was allowed to linearly interpolate between the profiles to create  $h(x)$ . For studies H1–H5, the mean of the variability  $m_{hx}=80$  m and the standard deviation of the variability  $s_{hx}$  were set as constants and defined as

$$m_{hx} = \frac{1}{N+1} \sum_{i=0}^N [h]_i, \quad (7)$$

$$s_{hx} = \pm \sqrt{\frac{1}{N+1} \sum_{i=0}^N ([h]_i - m_{hx})^2}. \quad (8)$$

TABLE III. Sample mean ( $m$ ) and sample standard deviation for the model parameter values of the compressional speed  $s_{NV}$  (studies V1–V8) and the water depth  $s_{NH}$  (studies H1–H5). The sample means can be compared to the set mean of the studies,  $m_{vx}=1677$  m/s for V1–V8 and  $m_{hx}=80$  m for H1–H5.

Study number	$m$ (m/s) of $V_p$	$s_{NV}$ (m/s)
V1	1668	$\pm 19$
V2	1660	$\pm 26$
V3	1655	$\pm 37$
V4	1694	$\pm 28$
V5	1680	$\pm 51$
V6	1691	$\pm 32$
V7	1672	$\pm 7$
V8	1675	$\pm 4$
Study number	$m$ (m) of $H$	$s_{NH}$ (m)
H1	79.8	$\pm 0.4$
H2	79.7	$\pm 0.5$
H3	79.6	$\pm 0.8$
H4	79.5	$\pm 1.1$
H5	79.6	$\pm 1.4$

The  $s_{hx}$  of Eq. (8) is equivalent to  $s_{hx}$  of Eq. (B9). The distance between environmental profiles in PECAN was  $10$  m.

On the left-hand side of Fig. 13, three realizations of the ocean bottom are shown, one realization from study H1 where  $s_{hx} = \pm 0.125$  m, one realization from study H3 where  $s_{hx} = \pm 0.5$  m, and one realization from H5 where  $s_{hx} = \pm 1$  m. It can be seen that for  $s_{hx} = \pm 0.125$  m the water depth barely deviates from the mean  $m_{hx}$ . The realizations of the ocean bottoms, such as those shown in Fig. 13, are a series of contiguous line segments, as mentioned earlier. As seen in the figure, the segments were small enough with respect to the entire range  $R$  that it made the realization of the ocean bottom appear to be smooth. On the right-hand side of Fig. 13 a histogram is shown of the slopes for each segment used to make each of the  $100$  realizations of the ocean bottoms for each of the three studies. For  $s_{hx} = \pm 0.125$  m, most segments have a slope within  $\pm 0.5^\circ$ . For  $s_{hx} = \pm 0.5$  m, most segments have a slope within  $\pm 1^\circ$ . For  $s_{hx} = \pm 1$  m, most segments have a slope within  $\pm 2^\circ$ . The distributions show no unexpected trends.

The two-dimensional correlation scatter plots for studies H1–H5 (not shown) had similar trends as for the variable compressional speed studies that allowed comparison be-

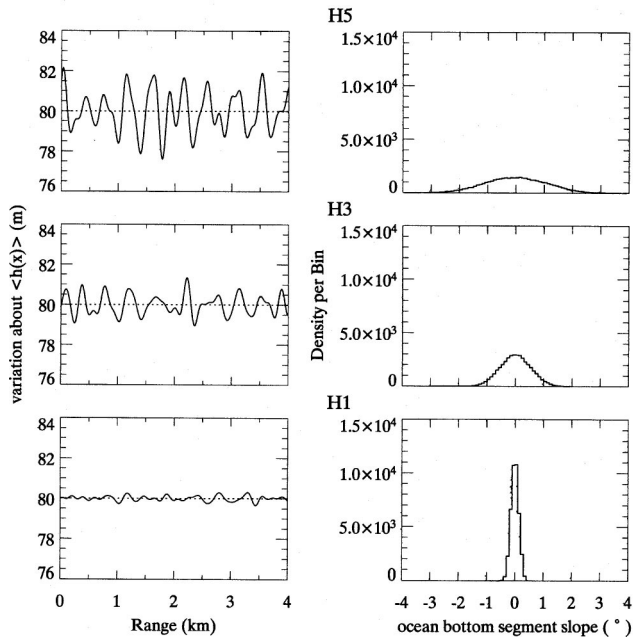


FIG. 13. Variable water depth. Sample realizations of the variable water depth are shown on the left-hand side for studies H1, H3, and H5. The dotted line represents the mean of the curve  $m_{hx}$ . On the right-hand side are histograms of all the slopes of the segments that make up each realization of the variable water depth used in the study.

tween different values of  $s_{vx}$  (Figs. 7–9). At  $s_{hx} = \pm 0.125$  m, all parameters have two dimensional correlations. As  $s_{hx}$  increases the correlations decrease until almost no correlations are visible at  $s_{hx} = \pm 1$  m, with the exception being a slight correlation between the  $V_p$  and  $H$ . The correlations that exist for low standard deviations again show the presence of a family of “effective” or nearly equivalent seabed models that can characterize the seabed.

Figure 14 shows the histograms for studies H1 [shown in Figs. 14(i)–14(l)], H3 [shown in Figs. 14(e)–14(h)], and H5 [shown in Figs. 14(a)–14(d)]. For  $s_{hx} = \pm 0.125$  m [Figs. 14(i)–14(l)], there is a concentration of solutions about the

true mean  $m_{hx}$  and true model parameter values but the concentration about these values decreases as  $s_{hx}$  increases. It appears that if one hopes to attain inversion results about the true or true mean values, then assuming a range-independent environment would be unwise for an  $s_{hx}$  value of 0.5 m or above, for this environment.

As was the case for sound speed, the effect of environmental variation of sound speed is striking. A shallow water seabed roughness of the order of 1 m is typical, as reported by Turgut *et al.*<sup>34</sup> for the New Jersey shelf. The results in this paper show that inversions in environments with typical values of water depth variance lead to significant uncertainty in all estimated parameter values, when environmental variability is ignored.

Table III reports the mean of the inversion solution parameter values for the variable water depth studies. Like for the variable compressional speed studies, the true mean of the studies,  $m_{hx}$ , always fell within one standard deviation of the mean of the inversion solution values for each study. And again, there was a difference from study to study between the values of  $s_{NH}$ , the standard deviation of the model parameter values for the water depth.

#### IV. CONCLUSIONS

Ignored variability in the environment can lead to significant uncertainty in the values of inversion parameters. Naively, one would hope that a single inversion of constant model parameters in a random environment would provide a confident estimate of the average environment, that is, the precise values of those parameters that do not vary and the mean values of those parameters that do vary. Typical experimental inversions of real ocean data implicitly make this assumption: it is impractical to model all the details of the random environment, so a simplified model with average parameters is devised, and the inversion is assumed to estimate those parameter values. This investigation has shown that matched-field geoacoustic inversion in variable environments is uncertain: the best-fit model of a single realization

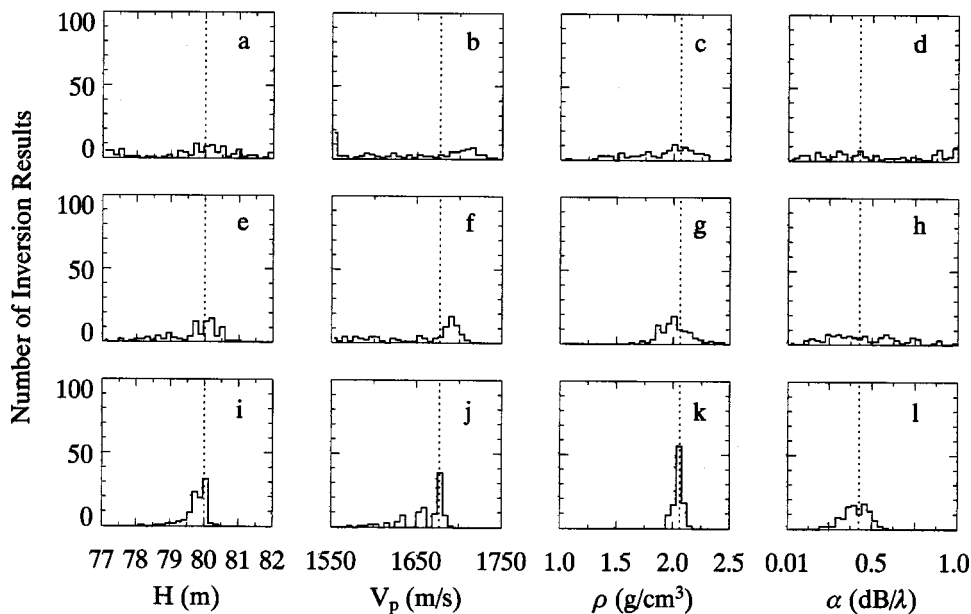


FIG. 14. Looking at the effects of variable water depth. The histograms of the inversion results are presented for studies H5 ( $s_{hx} = \pm 1.0$  m) shown in (a)–(d), H3 ( $s_{hx} = \pm 0.5$  m) shown in (e)–(h), and H1 ( $s_{hx} = \pm 0.125$  m) shown in (i)–(l). The inversion results include model parameter values for water depth  $H$ , compressional speed  $V_p$ , density  $\rho$ , and attenuation  $\alpha$ . For  $V_p$ ,  $\rho$ , and  $\alpha$  the vertical dotted lines represent the true model parameter values used to generate the measured acoustic field, and for  $H$  it represents the  $m_{hx}$ . The abscissa limits represent the bounds used in the inversions.

of the random environment does not necessarily reproduce the mean environment. The uncertainty is complex, that is, randomizing only one parameter in the environment leads to uncertainty in all parameters of the bestfit model. In addition, the uncertainty is structured, in that the variations of model parameters over all realizations of the random environment are correlated.

Looking at the statistics of the model parameter variations, it is clear (and no surprise) that the uncertainty of the inversions increases with the variability of the input model, regardless of which parameter is randomized. In many ways, the results are reminiscent of inversion of noisy acoustic data. The dependence of the inversion results on source-receiver range is weak, although there is some suggestion that there is more spread in inverted parameter values at longer ranges. Inversion performance improves with increasing frequency, likely due to there being more independent information at the hydrophone elements. Performance improves again when data from two frequencies are jointly inverted.

Looking at the pairwise scatter plots of inverted parameters, it is evident that the inverted parameters are strongly correlated, although the correlation weakens with increasing variability of the environment. This implies that the random-environment inversion problem is somewhat overdetermined by the chosen model parametrization; that is, the best-fit models form a family that represents an effective seabed model having simpler characteristics.

Although this investigation is not comprehensive, the results obtained indicate that a single inversion of a random environment would not confidently characterize the mean environment, although it would provide parameter values for a plausible model environment that matches the data within reasonable error bounds.

## ACKNOWLEDGMENTS

The authors would like to thank Ron Kessel for his discussions, insights and inputs concerning this work.

## APPENDIX A: CALCULATING MEAN AND STANDARD DEVIATION FOR $v(x)$

For variable compressional speed, to create  $v_p(x)$ , fluctuations were generated using scaled pseudorandom numbers picked from a uniform distribution. For  $N+1$  fluctuations,  $N+1$  pseudorandom numbers were generated and then linearly interpolated to form a line-form such as the one illustrated in Fig. 2. To keep control over the statistics of the line-forms the mean and standard deviation needed to be derived. This appendix outlines the derivation used.

Given a function  $f(x)$ , as illustrated in Fig. 15, defined on  $[0, R]$ , formed by connecting  $N+1$  random numbers  $\{y_i, i=0, N\}$  picked from a uniform distribution, then the global mean of  $f(x)$  can be defined as

$$m_{fx} = \frac{1}{R} \int_0^R f(x) dx = \frac{1}{R} \sum_{i=0}^N \int_{x_i}^{x_{i+1}} f(x) dx, \quad (A1)$$

where  $x_0=0$  and  $x_{N+1}=R$ . Let,

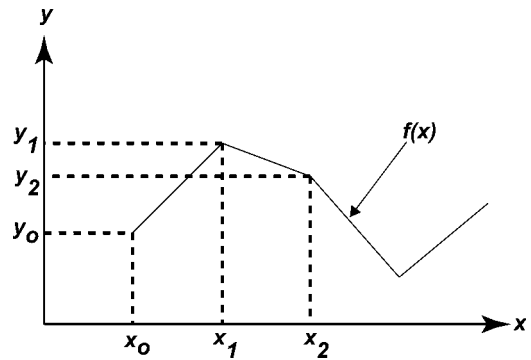


FIG. 15. Schematic representation of a line-form function [similar to  $v_p(x)$ ] used to help clarify the derivation of the global mean and standard deviation of  $f(x)$  in Appendix A.

$$f(x) = y = \left( \frac{y_{i+1} - y_i}{x_{i+1} - x_i} \right) (x - x_i) + y_i; \quad (A2)$$

therefore,

$$x = (y - y_i) \left( \frac{x_{i+1} - x_i}{y_{i+1} - y_i} \right) + x_i \quad (A3)$$

and

$$\frac{dx}{dy} = \left( \frac{x_{i+1} - x_i}{y_{i+1} - y_i} \right), \quad (A4)$$

$$dx = \left( \frac{x_{i+1} - x_i}{y_{i+1} - y_i} \right) dy. \quad (A5)$$

Given that  $f(x_i) = y_i$  then substituting Eq. (A5) into Eq. (A1) and substituting  $y$  for  $f(x)$  gives

$$m_{fx} = \frac{1}{R} \sum_{i=0}^N \int_{y_i}^{y_{i+1}} y \left( \frac{x_{i+1} - x_i}{y_{i+1} - y_i} \right) dy. \quad (A6)$$

If  $x_{i+1} - x_i = \Delta x$ , as is the case in this work, and given that  $\Delta x/R = 1/N$  then Eq. (A6) solves to be

$$m_{fx} = \frac{\Delta x}{R} \sum_{i=0}^N \frac{y_{i+1}^2 - y_i^2}{2(y_{i+1} - y_i)} = \frac{1}{2N} \sum_{i=0}^N (y_{i+1} + y_i). \quad (A7)$$

Equation (A7) is therefore the global mean for the line-form  $f(x)$ .

Similarly, the square of the standard deviation  $s_{fx}$  for the line-form  $f(x)$  can be derived thus,

$$\begin{aligned} s_{fx}^2 &= \frac{1}{R} \int_0^R (f(x) - m_{fx})^2 dx \\ &= \frac{1}{R} \sum_{i=0}^N \int_{x_i}^{x_{i+1}} (f(x) - m_{fx})^2 dx \\ &= \frac{1}{R} \sum_{i=0}^N \int_{y_i}^{y_{i+1}} (y - m_{fx})^2 \frac{x_{i+1} - x_i}{(y_{i+1} - y_i)} dy \\ &= -m_{fx}^2 + \frac{\Delta x}{3R} \sum_{i=0}^N \frac{(y_{i+1}^3 - y_i^3)}{(y_{i+1} - y_i)} \\ &= -m_{fx}^2 + \frac{1}{3N} \sum_{i=0}^N (y_{i+1}^2 + y_i^2 + y_{i+1}y_i). \end{aligned} \quad (A8)$$

## APPENDIX B: VARIABLE WATER DEPTH

For modeling purposes, the seabed height is simulated as a random process based on observed power-law wavenumber spectra. Let

$$\hat{h}(x) = \int_{-\infty}^{+\infty} S(k) e^{ikx} dk, \quad (\text{B1})$$

in which  $\hat{h}(x)$  is the height of the seabed above the mean level [i.e.,  $\hat{h}(x) + m_{hx} = h(x)$ ],  $x$  is the distance along the track,  $k$  is the wave number ( $k = 2\pi/\lambda$ ),  $\lambda$  is the wavelength, and  $S(k)$  is the Fourier transform of  $\hat{h}(x)$ .

Since  $\hat{h}(x)$  is real, it is necessary that

$$S(-k) = S^*(k), \quad (\text{B2})$$

where  $*$  indicates the complex conjugate. It is convenient to represent  $S(k)$  in polar form, that is,

$$S(k) = |S(k)| e^{i\phi(k)}, \quad (\text{B3})$$

in which case the phase function  $\phi(k)$  must have the symmetry

$$\phi(-k) = -\phi(k), \quad (\text{B4})$$

so that Eq. (B2) is satisfied. Then Eq. (B1) becomes

$$\hat{h}(x) = 2 \int_0^{+\infty} |S(k)| \cos[kx + \phi(k)] dk. \quad (\text{B5})$$

The covariance of the surface is

$$\begin{aligned} C(x) &= \int_{-\infty}^{+\infty} \hat{h}(x') \hat{h}(x' + x) dx' \\ &= 2 \int_0^{+\infty} |S(k)|^2 \cos(kx) dk. \end{aligned} \quad (\text{B6})$$

Note that the covariance is independent of the phase function, and that the spectrum  $|S(k)|^2$  is the Fourier transform of the covariance  $C(x)$ . By randomly choosing different phase functions, it is possible to create multiple realizations of a rough surface having uniform covariance and spectrum.

The square of the standard deviation of the surface height is simply

$$\sigma^2 = C(0) = 2 \int_0^{+\infty} |S(k)|^2 dk, \quad (\text{B7})$$

that is, the area under the spectrum.

To implement this in simulations, we employ a finite sum over sinusoids having discrete wave numbers  $k_n \in \{k_1, k_2, k_3, \dots, k_N\}$ , specified amplitudes  $A_n \in \{A_1, A_2, A_3, \dots, A_N\}$ , and random phases  $\phi_n \in \{\phi_1, \phi_2, \phi_3, \dots, \phi_N\}$ . That is,

$$\hat{h}(x) \approx \sum_{n=1}^N A_n \cos(k_n x + \phi_n). \quad (\text{B8})$$

We need to choose the wave numbers, amplitudes, and phases to generate a seabed with the correct statistics.

The square of the standard deviation from Eq. (B8) is

$$s_{hx}^2 \approx \frac{1}{2} \sum_{n=1}^N A_n^2 \approx \sigma^2 \quad (\text{B9})$$

so it seems that  $A_n^2$  plays the same role as  $|S(k)|^2 dk$ .

Observations have shown<sup>35,36</sup> that seabed roughness spectra can be described in a power-law form:

$$|S(k)|^2 \propto k^{-b} (b > 1), \quad (\text{B10})$$

such that long wavelengths (low wave numbers) have higher amplitudes than short wavelengths (high wave numbers). In order that the integral in Eq. (B7) and the sum in Eq. (B9) be finite. It is necessary that the band of wave numbers be limited, at least at the lower end; that is,

$$k_{\min} < k < k_{\max}. \quad (\text{B11})$$

Since  $A_n^2$  plays the same role as  $|S(k)|^2 dk$ , we propose that the amplitudes be given by

$$A_n = \sqrt{a k_n^{-b} \Delta k_n}, \quad (\text{B12})$$

in which

$$a \approx \frac{2s_{hx}^2}{\sum_{i=1}^N k_i^{-b} \Delta k_i} \quad (\text{B13})$$

and

$$\Delta k_n = \frac{1}{2}(k_{n+1} - k_{n-1}). \quad (\text{B14})$$

It remains to choose the actual distribution of wave numbers. We propose that the wave numbers be distributed unevenly, progressively choosing more at the lower range, to minimize the number needed. One approach is to define the sequence

$$k_n = \alpha^{n-1} k_1, \quad (\text{B15})$$

in which

$$k_1 \equiv k_{\min} \equiv 2\pi/\lambda_{\max}, \quad (\text{B16})$$

$$k_N \equiv k_{\max}, \quad (\text{B17})$$

and  $\alpha$  is a factor to be determined. Let  $k_N$  be the wave number at which the spectrum  $|S(k)|^2$  is some fraction  $\beta$  of its value at  $k_1$ , that is,

$$\beta = \left( \frac{k_1}{k_N} \right)^b \quad (\text{B18})$$

then, from Eq. (B15),

$$\alpha = \beta^{-1/[b(N-1)]}. \quad (\text{B19})$$

Here is the procedure to synthesize a rough seabed: choose a standard deviation of the surface height  $s_{hx}$  (say, 0.5 m), a power-law exponent  $b$  (2–3 is typical), a maximum wavelength  $\lambda_{\max}$ , the number of sinusoidal components  $N$  (say, 10), and a value for  $\beta$  (say, 1/20). Then calculate  $\alpha$  from Eq. (B19),  $k_1$  from Eq. (B16), and the other  $k_n$  from Eq. (B15). From the wave numbers, calculate the  $\Delta k_n$  from Eq. (B14), and then the  $A_n$  from Eqs. (B12) and (B13). Then choose a set of phases  $\{\phi_1, \phi_2, \phi_3, \dots, \phi_N\}$  randomly distributed over an interval of  $2\pi$  radians. Finally, calculate the random seabed function  $\hat{h}(x)$  from Eq. (B8). Different sets of random phases will generate different realizations of the seabed having the same statistics. It is prudent to calculate

$s_{hx}$  from the final result to verify that it has the value one started with. The method of synthesizing roughness profiles using discrete sine waves was adapted from the synthesis of ocean surface wave forms.<sup>37</sup> The parameter values used in this study are:  $\lambda_{\max}=500$  m,  $N=9$ ,  $b=3$ , and  $\beta=0.05$ . This combination of values generates plausible synthetic realizations of seabed topography with reproducible statistics.

- <sup>1</sup>S. E. Dosso, M. J. Wilmut, and A. S. Lapinski, "An adaptive hybrid algorithm for geoaoustic inversion," *IEEE J. Ocean. Eng.* **26**, 324–336 (2001).
- <sup>2</sup>M. R. Fallat and S. E. Dosso, "Geoacoustic inversion via local, global and hybrid algorithms," *J. Acoust. Soc. Am.* **105**, 3219–3230 (1999).
- <sup>3</sup>P. Gerstoft, "Inversion of acoustic data using a combination of genetic algorithms and the Gauss-Newton approach," *J. Acoust. Soc. Am.* **97**, 2181–2190 (1995).
- <sup>4</sup>M. D. Collins, W. A. Kuperman, and H. Schmidt, "Nonlinear inversion for ocean-bottom properties," *J. Acoust. Soc. Am.* **92**, 2770–2783 (1992).
- <sup>5</sup>G. J. Heard, D. Hannay, and S. Carr, "Genetic algorithm inversion of the 1997 Geoacoustic Inversion Workshop test case data," *J. Comput. Acoust.* **6**, 61–71 (1998).
- <sup>6</sup>P. Ratilal, P. Gerstoft, and J. T. Goh, "Subspace approach to inversion by genetic algorithms involving multiple frequencies," *J. Comput. Acoust.* **6**, 99–115 (1998).
- <sup>7</sup>S. D. Rajan, J. F. Lynch, and G. V. Frisk, "Perturbative inversion methods for obtaining bottom geoacoustic parameters in shallow water," *J. Acoust. Soc. Am.* **82**, 998–1017 (1987).
- <sup>8</sup>A. Tolstoy, "MFP benchmark inversions via the RIGS method," *J. Comput. Acoust.* **6**, 185–203 (1998).
- <sup>9</sup>N. R. Chapman, S. Chin-Bing, D. King, and R. B. Evans, "Benchmarking geoacoustic inversion methods for range-dependent waveguides," *IEEE J. Ocean. Eng.* **28**, 320–330 (2003).
- <sup>10</sup>G. H. Brooke, D. J. Thomson, and G. R. Ebbeson, "PECAN: A Canadian parabolic equation model for underwater sound propagation," *J. Comput. Acoust.* **9**, 69–100 (2001).
- <sup>11</sup>A. S. Lapinski and S. E. Dosso, "Bayesian geoacoustic inversion for the Inversion Techniques 2001 Workshop," *IEEE J. Ocean. Eng.* **28**, 380–393 (2003).
- <sup>12</sup>P. L. Nielsen, M. Siderius, and P. Gerstoft, "Range-dependent geoacoustic inversion: Results from the inversion techniques workshop," *IEEE J. Ocean. Eng.* **28**, 414–423 (2003).
- <sup>13</sup>C. H. Harrison and M. Siderius, "Effective parameters for matched field geoacoustic inversion in range-dependent environments," *IEEE J. Ocean. Eng.* **28**, 432–445 (2003).
- <sup>14</sup>M. Siderius, P. L. Nielsen, and P. Gerstoft, "Range-dependent seabed characterization by inversion of acoustic data from a towed receiver array," *J. Acoust. Soc. Am.* **112**, 1523–1535 (2002).
- <sup>15</sup>M. R. Fallat, S. E. Dosso, and P. L. Nielsen, "An investigation of algorithm-induced variability in geoacoustic inversion," *IEEE J. Ocean. Eng.* **29**, 78–87 (2004).
- <sup>16</sup>D. M. F. Chapman and D. D. Ellis, "Propagation loss modelling on the Scotian Shelf: the geo-acoustic model," in *Bottom-Interacting Ocean Acoustics*, edited by W. A. Kuperman and F. B. Jensen (Plenum, New York, 1980); the proceedings of a conference held at SAACLANTCEN, La Spezia, Italy, June 1980.
- <sup>17</sup>D. D. Ellis and D. M. F. Chapman, "Propagation loss modelling on the Scotian Shelf: comparison of model predictions with experiment," in *Bottom-Interacting Ocean Acoustics*, W. A. Kuperman and F. B. Jensen, eds. (Plenum Press, New York, 1980); the proceedings of a conference held at SAACLANTCEN, La Spezia, Italy, June 1980.
- <sup>18</sup>A. G. McKay, J. A. Hunter, R. L. Good, and D. M. F. Chapman, "A 12-channel marine EEL for shallow refraction surveying of the seabottom in coastal waters," in *Ocean Seismo-Acoustics*, edited by T. Akal and J. M. Berson (Plenum, New York, 1986), pp. 871–880.
- <sup>19</sup>J. C. Osler, "A geo-acoustic and oceanographic description of several shallow water experimental sites on the scotian shelf," DREA Technical Memorandum 94/216 [Defence Research Establishment Atlantic (now Defence Research Development Canada—Atlantic), Dartmouth, Nova Scotia, 1994].
- <sup>20</sup>E.-L. Hamilton, "Geoacoustic modeling of the sea floor," *J. Acoust. Soc. Am.* **68**, 1313–1340 (1980).
- <sup>21</sup>S. E. Dosso and M. J. Wilmut, "Effects of incoherent and coherent source spectral information in geoacoustic inversion," *J. Acoust. Soc. Am.* **112**, 1390–1398 (2002).
- <sup>22</sup>C. F. Mecklenbrauker and P. Gerstoft, "Objective functions for ocean acoustic inversion derived by likelihood methods," *J. Comput. Acoust.* **8**, 259–270 (2000).
- <sup>23</sup>J. A. Nelder and R. Mead, "A simplex method for function minimization," *Comput. J.* **7**, 308–313 (1965).
- <sup>24</sup>W. H. Press, S. A. Teukolsky, W. T. Vetterling, and B. P. Flannery, *Numerical Recipes*, 2nd ed. (Cambridge University Press, Cambridge, 1992).
- <sup>25</sup>S. Kirkpatrick, C. D. Gelatt, Jr., and M. P. Vecchi, "Optimization by simulated annealing," *Science* **220**, 671–680 (1983).
- <sup>26</sup>N. Metropolis, A. Rosenbluth, M. Rosenbluth, A. Teller, and E. Teller, "Equation of state calculation by fast computing machines," *J. Chem. Phys.* **21**, 1087–1092 (1953).
- <sup>27</sup>D. M. F. Chapman, "What are we inverting for?," in *Inverse Problems in Underwater Acoustics*, edited by M. I. Taroudakis and G. N. Makrakis (Springer, New York, 2001), pp. 1–14.
- <sup>28</sup>S. E. Dosso, "Quantifying uncertainty in geoacoustic inversion. I. A fast Gibbs sampler approach," *J. Acoust. Soc. Am.* **111**, 129–142 (2002).
- <sup>29</sup>L. A. Mayer, B. J. Kraft, P. Simpkin, P. Lavoie, E. Jabs, and E. Lynskey, "In-situ determination of the variability of seafloor acoustic properties: an example from the ONR geoclutter area," in *Impact of Littoral Environmental Variability on Acoustic Predictions and Sonar Performance*, edited by N. G. Pace and F. B. Jensen (Kluwer, Dordrecht, 2002), pp. 115–122.
- <sup>30</sup>K. D. Lepage, "Modeling propagation and reverberation sensitivity to oceanographic and seabed variability," in Ref. 29, pp. 353–360.
- <sup>31</sup>M. D. Collins, W. A. Kuperman, and H. Schmidt, "Nonlinear inversion for ocean-bottom properties," *J. Acoust. Soc. Am.* **92**, 2770–2783 (1992).
- <sup>32</sup>P. Ratilal, P. Gerstoft, and J. T. Goh, "Subspace approach to inversion by genetic algorithms involving multiple frequencies," *J. Comput. Acoust.* **6**, 99–115 (1998).
- <sup>33</sup>M. I. Taroudakis and M. G. Markaki, "Bottom geoacoustic inversion by matched field processing—A sensitivity study," *Inverse Probl.* **16**, 1679–1692 (2000).
- <sup>34</sup>A. Turgut, D. Lavoie, D. J. Walter, and W. B. Sawyer, "Measurements of bottom variability during SWAT New Jersey shelf experiments," in Ref. 29, pp. 91–98.
- <sup>35</sup>J. M. Berkson and J. E. Mathews, "Statistical properties of sea-floor roughness," in *Acoustics and the Seabed*, edited by N. G. Pace (Bath University Press, Bath, UK, 1983), pp. 215–223.
- <sup>36</sup>K. B. Briggs, D. Tang, and K. L. Williams, "Characterization of interface roughness of rippled sand off Fort Walton Beach, Florida," *IEEE J. Ocean. Eng.* **27**, 505–514 (2002).
- <sup>37</sup>J. P. Brett, "Computer-generated random sea surfaces for use with the program CABUOY," Naval Air Development Center Technical Memorandum 2063-TM-46-77, July, 1977.